JMEPEG (2014) 23:3305–3313
DOI: 10.1007/s11665-014-1123-4

1059-9495/$19.00

The Microstructure Degradation of the IN 713C Nickel-Based Superalloy After the Stress Rupture Tests

Hubert Matysiak, Malgorzata Zagorska, Alicja Balkowiec, Boguslawa Adamczyk-Cieslak, Rafal Cygan, Jan Cwajna, Jacek Nawrocki, and Krzysztof J. Kurzydłowski

(Submitted April 23, 2014; in revised form May 20, 2014; published online June 27, 2014)

The aim of the work was to examine the degradation phenomena taking place in the microstructure of the as-cast IN 713C superalloy after stress rupture tests, performed at $T = 980$ °C under a tensile stress of 150 MPa. A directional growth of γ' phase (rafting) and decomposition of the NbC primary carbides accompanied by the precipitation of $M_{23}C_6$ secondary carbides rich in chromium and of γ' phase were observed. It was also indicated that the decomposition of the NbC primary carbides may be accompanied by the precipitation of M_3B_2 borides rich in Mo.

Keywords IN 713C superalloy, investment casting, M_3B_2 boride, MC degradation, microstructure of casts, stress rupture test

1. Introduction

IN 713C nickel superalloy was developed by the International Nickel Company in the 1950s (Ref 1). It was initially designed for air melting and casting under the protection of inert gases. However, relatively soon, it was discovered that the maximum of mechanical properties was reached when the casts were manufactured with the use of vacuum casting techniques. The alloy proved to possess a very good castability, good mechanical properties at elevated temperatures, and a high stability of the microstructure while being available at an acceptable price (Ref 1-9). The cost which is a very significant aspect (from the economical point of view) derives from the fact that the alloy does not contain the expensive cobalt.

Despite the passage of time, IN 713C is still commonly employed in the aircraft industry for the production of engine turbine parts, mainly in the low pressure section (LPT). For example, the designers of the large aircraft turbofan engine GP7200 selected this alloy for the production of LPT blades and LPT vane clusters. These complicated castings must meet all the quality requirements, which, in this case, are highly strict. Every IN 713C superalloy master ingot has to undergo tests concerning the chemical composition (investigating the content of the main alloying elements and the trace elements). Moreover, each ingot needs to withstand the analysis of the mechanical properties of static tensile test at elevated temperature and stress rupture tests. The stress rupture tests are carried out at 980 °C, which significantly exceed the in-service requirements of the cast. Thus, the aim of the present study was to examine the phenomena of microstructural degradation of the as-cast IN 713C superalloy, taking place during stress rupture tests.

2. Material for Investigations and Experimental Procedure

The tested material was the IN 713C nickel superalloy with the chemical composition as shown in Table 1. The as-received material was melted and investment cast under the following conditions: melt pouring temperature $T_m = 1500$ °C, shell mold preheat temperature, $T_s = 1200$ °C, vacuum level 10^{-3} mbar. The cast bar blanks were machined into cylindrical geometry specimens. The geometry of the sample for the stress rupture tests is presented in Fig. 1. Stress rupture tests were performed in accordance with ASTM E139 standard under 980 °C/150 MPa in air. The results for all tested samples confirmed that time to rupture is longer than 25 h (average $t = 26.5 \pm 1$ h), and the elongation till rupture equaled $A = 5\%$; therefore, the outcome meets the requirements of the industrial standards.

Microstructure observations and analyses of the as-cast IN 713C and IN 713C after the stress rupture tests were carried out by scanning (SEM) and transmission electron microscopy (TEM). The SEM specimens were prepared using a standard procedure for metallographic preparation. Plasma cleaning was carried out prior to loading the sample into the SEM microscope in order to protect carbon contamination. The specimens were analyzed by FE SEM Hitachi SU70 field emission microscope equipped with energy dispersive x-ray spectroscopy (EDS). For the imaging and EDS analyses, a 15 kV accelerating voltage was used.

Hubert Matysiak, Functional Materials Research Center, Warsaw University of Technology, Woloska 141, 02-507 Warsaw, Poland; **Malgorzata Zagorska, Alicja Balkowiec, Boguslawa Adamczyk-Cieslak,** and **Krzysztof J. Kurzydłowski**, Faculty of Materials Science and Engineering, Warsaw University of Technology, Woloska 141, 02-507 Warsaw, Poland; **Rafal Cygan,** Wytwornia Sprzetu Komunikacyjnego, "PZL Rzeszow" S.A., Hetmanska 120, 35-078 Rzeszow, Poland; **Jan Cwajna,** Faculty of Materials Engineering and Metallurgy, Silesian University of Technology, Krasińskiego 8, 40-019 Katowice, Poland; and **Jacek Nawrocki,** Faculty of Mechanical Engineering and Aeronautics, Rzeszow University of Technology, Al. Powstancow Warszawy 8, 35-959 Rzeszow, Poland. Contact e-mail: m.zagorska@inmat.pw.edu.pl.

Table 1 Chemical composition of IN 713C superalloy

Element	C	Si	B	Al	Ti	Nb	Mo	Cr	Fe	Zr	Ni
wt.%	0.096	0.010	0.010	6.080	0.840	2.160	4.210	13.580	0.090	0.060	Remainder

Samples for TEM observations were prepared using a single focused ion beam (FIB) system (Hitachi FB-2100) and lift-out preparation technique. TEM microstructure investigations were performed using a Jeol JEM 1200EX II (operating at 120 kV) microscope equipped with the EDS device.

3. Results

Figure 2 and 3 show the typical SEM images of the IN 713C superalloy microstructure, in the as-cast state and after the stress rupture test. Figure 2(a) presents the typical cubic morphology of γ'- $Ni_3(Al,Ti)$ phase in the γ phase matrix (nickel-based solid solution) for the as-cast IN 713C superalloy (Ref 1), whereas Fig. 2(b) shows the directional morphology (rafting) of γ' phase (Ref 10-12) in the IN 713C superalloy after the stress rupture tests.

Figure 3(a) and (e) presents SEM images of MC primary carbides rich in Nb (chemical composition shown in Fig. 4a) (Ref 2, 3) in the IN 713C superalloy in the as-cast state and after the stress rupture test. The NbC primary carbides precipitate in the interdendritic areas of the as-cast state occur in forms of irregular particles, Chinese script forms, and (γ/NbC) eutectic, as shown in Fig. 3(a), (b), and (f), respectively. After the stress rupture test, the density and size of the MC carbides in the interdendritic areas are significantly lower.

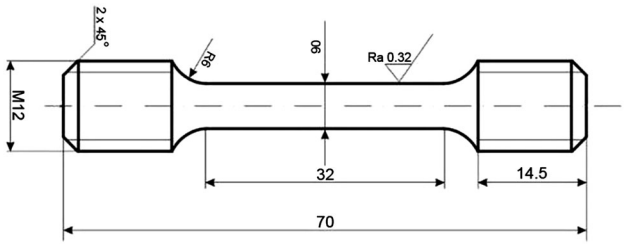

Fig. 1 Geometry of the sample for stress rupture tests (mm)

Moreover, interdendritic areas free of NbC are observed, which prove their dissolution. At a large magnification (Fig. 3f and g), in the NbC dissolution areas, the presence of a phase rich in Cr was detected (spectrogram in Fig. 4b), as well as a phase rich in Mo (spectrogram in Fig. 4c) and γ' phase. A phase rich in Mo was also observed in the eutectic pools shown in Fig. 3(b), (d), and (h). In the eutectic, the phase rich in Ni and Zr (spectrogram in Fig. 4d) and γ phase were found. The typical primary (coarse) γ' phase (Ref 13) and (γ/γ') eutectic (Ref 2), precipitated in the interdendritic areas, were also observed, as shown in Fig. 3(c) and (d), respectively.

Figure 5(a) and 6(a) show TEM images of the IN 713C superalloy microstructure after the stress rupture tests, in the area of the dissolution of the primary carbide, with marked electron diffraction analysis areas. The obtained electron diffraction patterns are shown in Fig. 5(b) and 6(b) and compiled in Table 2. The patterns prove the presence of the following phases: primary carbide MC rich in Nb, γ and γ' phases, and $M_{23}C_6$ secondary carbides (rich in Cr). All those phases exhibit the commonly observed "cube-cube" crystallographic relationship (Ref 14), presented in Fig. 5(b) and 6(b).

Figure 7 shows the microstructure (TEM image) of the eutectic area, with marked electron diffraction analysis areas. The results of the obtained electronograms are compiled in Table 2. On their basis, it can be stated that the phase rich in Mo is a M_3B_2 boride, whereas the phase rich in Ni and Zr is Ni_7Zr_2. It was also proven that the crystallographic directions $[010]M_3B_2$ and $[21-1]Ni_7Zr_2$ are parallel—see Fig. 8g. One should also emphasize the good agreement of the measure of values of the interplanar spacings for phases γ, γ', $M_{23}C_6$, NbC, Ni_7Zr_2, and M_3B_2 with the data included in the powder diffraction files (PDF).

4. Discussion of the Results

The phenomenon of a directional growth (rafting) of γ' phase is often observed in the nickel superalloys at temperatures over

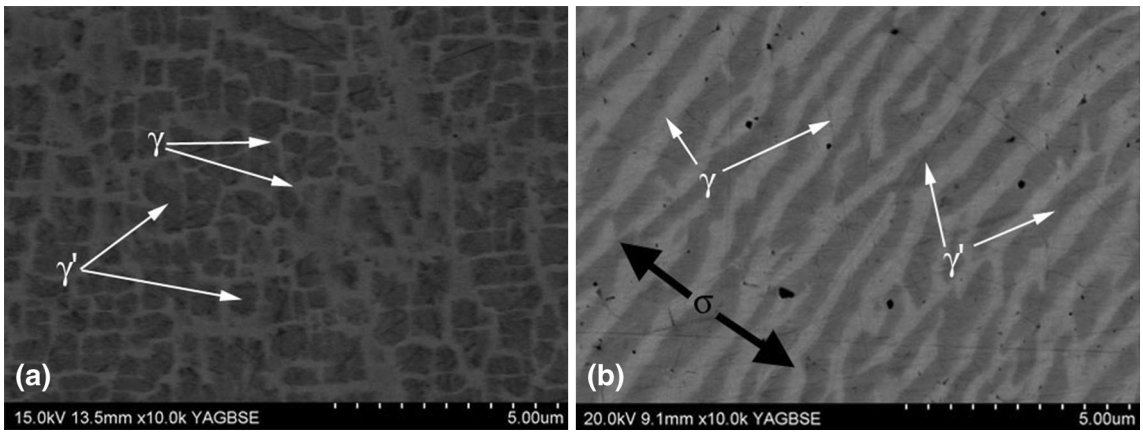

Fig. 2 The morphology of γ' phase IN 713C superalloy in the as-cast state (a) and after the stress rupture tests (b)

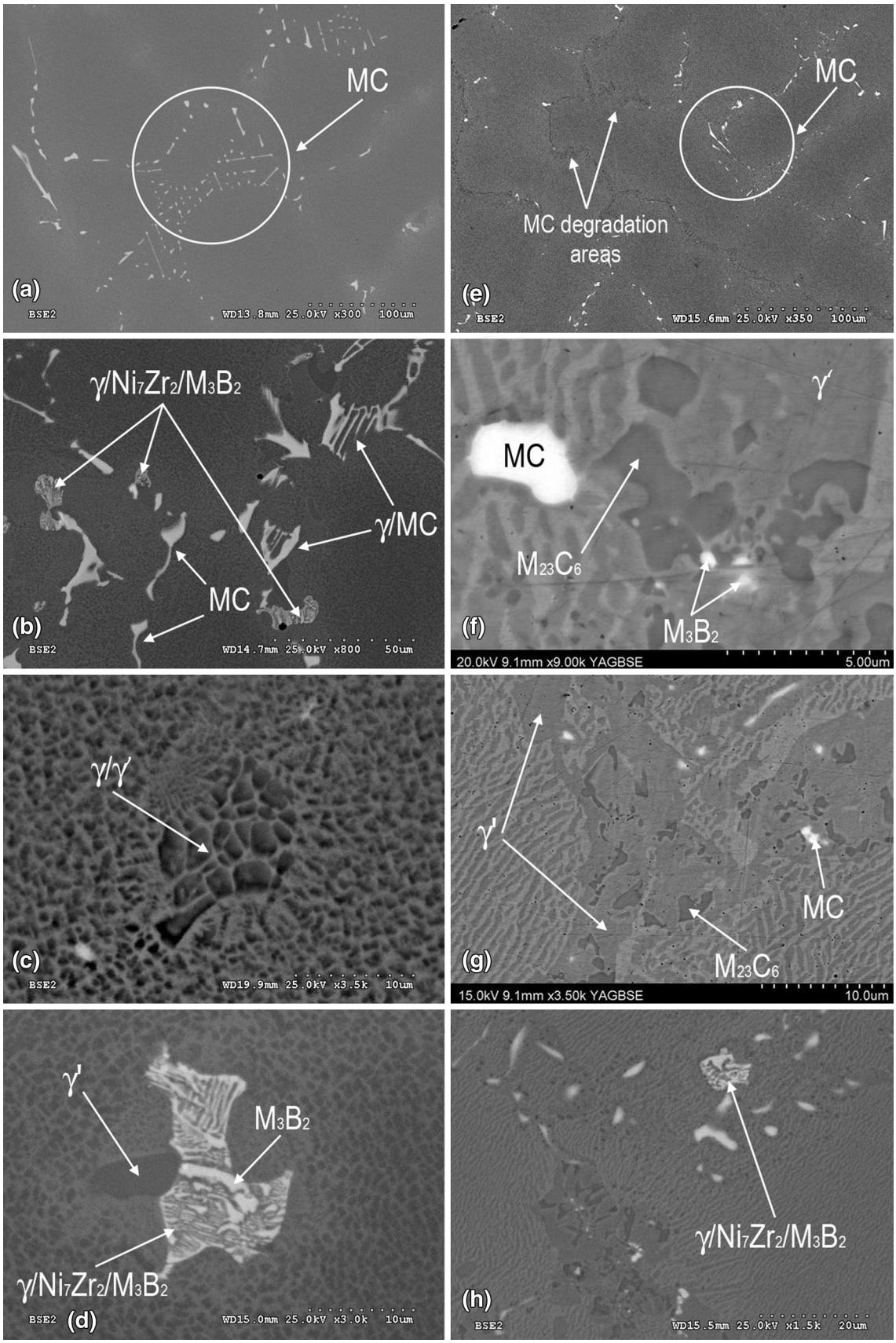

Fig. 3 SEM images in BSE electron contrast of the microstructure of superalloy IN 713C in the as-cast (a-d) and after stress rupture test (e-h), massive samples

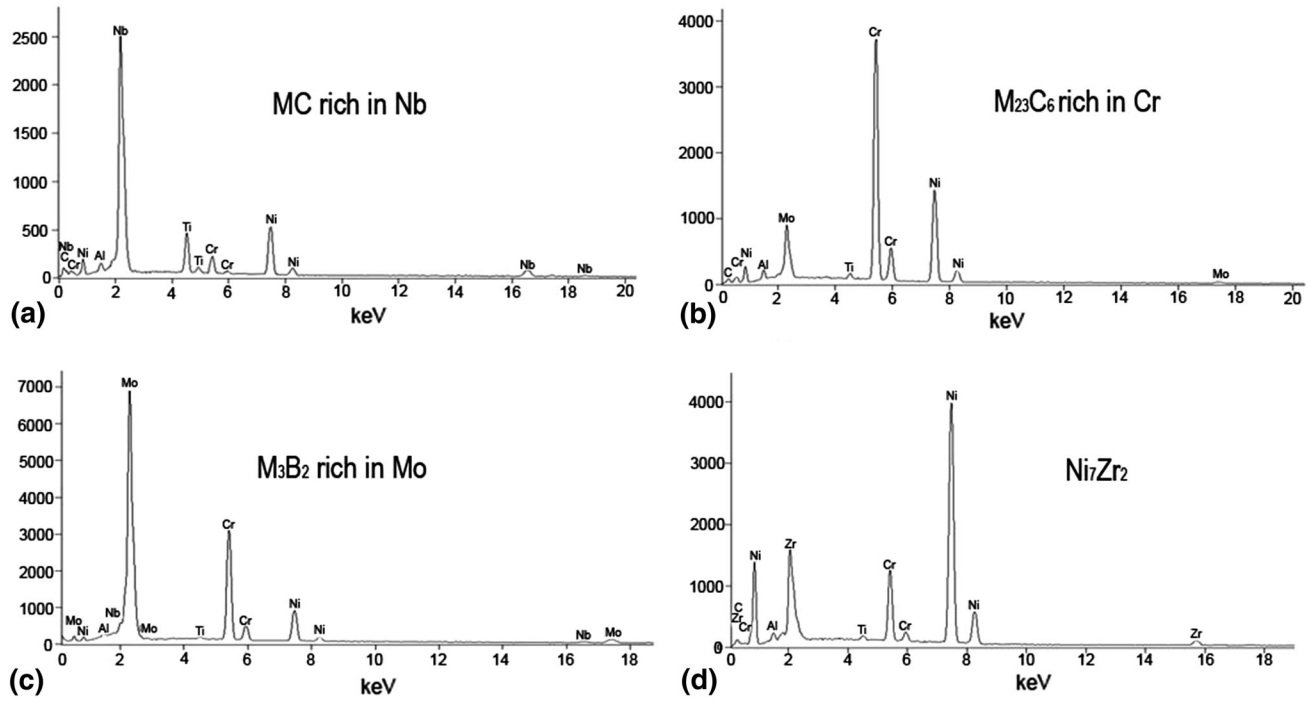

Fig. 4 Typical spectrograms for NbC (a), Ni_7Zr_2 (b), M_3B_2 (c), and $M_{23}C_6$ (d)

900 °C under the external stress. The process of a directional growth of phase γ′ is governed by (a) the value and the direction of the applied external stress, (b) the value and sign of the γ and γ′ lattice misfit (defined as $\delta = 2(a\gamma' - a\gamma)/(a\gamma' + a\gamma)$), where $a\gamma'$ and $a\gamma$ are lattices constant γ′ and γ, respectively), and (c) the elastic constants of γ and γ′ phases (Ref 10-12).

From the experimental observations (Ref 10-12) (in the case when γ and γ′ lattice misfits possess a negative misfit, the sample is tensile by the external stress), it can be concluded that the rafting is a sequential process. At first, a plastic deformation of the superalloy matrix occurs, which causes a loss of coherency at the γ and γ′ interfaces and a subsequent reduction of the misfit stress. All the internal stress components combine to yield one specific value for the hydrostatic stress. Tensile stresses act in the γ′ precipitates parallel to the γ-channels. These forces are balanced by compressive stresses in the γ-channels surfaces which are much higher than low tensile stress components which act perpendicularly to the channels. Perpendicular to the external stress axis, internal stresses change due to the different Poisson numbers of γ and γ′ phases. Therefore, the effective stress in the perpendicular γ channels is greater than in the parallel channels. This promotes diffusion processes as well as creep dislocation motion in the perpendicular channels and relaxes the internal stresses in these channels thus stabilizing the microstructure. The result is the rafting perpendicular to the external tensile γ′.

The lattice constants of γ′ and γ given in PDF 18-0872 and PDF 47-1417 (the best fit for the phases in the examined alloy) equal $a\gamma' = 3.5810$ Å and $a\gamma = 3.5975$ Å, respectively. This implies that δ is negative as for most nickel superalloys (equals −0.005). The observed directional growth of γ′ phase is of the N-type, in which the lamellae of γ′ phase are perpendicular to the tensile stress direction, and lattice misfit is negative. The P-type directional growth of γ′ phase (the lamellae of phase γ′ are perpendicular to the direction of force operation) occurs when external stresses are compressive, or the γ′ and γ lattice misfits have a positive value (Ref 10-12).

The SEM and TEM observations performed in the degradation area of the MC primary carbides suggest that, at the test temperature of 980 °C, the carbides are unstable and undergo decomposition. The most commonly observed mechanism of MC carbide degradation is described by reactions (Ref 15, 16):

$$\mathrm{MC} + \gamma \xrightarrow{T,t} \mathrm{M_{23}C_6} + \gamma', \text{ in our study : } (\mathrm{Nb,Ti})\mathrm{C} + (\mathrm{Ni,Mo,Cr,\ Ti,\ Al}) \rightarrow (\mathrm{Cr,Mo})_{23}\mathrm{C_6} + \mathrm{Ni_3(Al,Ti)} + \mathrm{Nb} \quad \text{(Eq 1)}$$

and

$$\mathrm{MC} + \gamma \xrightarrow{T,t} \mathrm{M_6C} + \gamma', \text{ which was not observed in our study} \quad \text{(Eq 2)}$$

As a result of reaction 1, we observed γ′ phase as well as the formation of $M_{23}C_6$ secondary carbides (rich in Cr). Additionally, the solid solution γ phase is enriched with Nb in the area of the NbC decomposition.

In reaction 2, in many nickel superalloys, M_6C secondary carbides are formed, rich in Mo, W, Co, Cr and Fe, which were not observed in this study. However, on the basis of the electron microscopic observations, it was proven that the phase rich in Mo, existing both in the area of NbC carbides dissolution and in the eutectic, is a M_3B_2 boride.

The present results indicate that the eutectic of the alloy consisted of γ, M_3B_2, and a phase rich in Ni-Zr. From the analysis of the phase equilibrium system (Ref 17) of the binary alloy Ni-Zr, it can be clearly stated that only one eutectic reaction occurs at 1170 °C, in which $L \rightarrow \gamma + Ni_5Zr$. This stands in clear contrast with our observations.

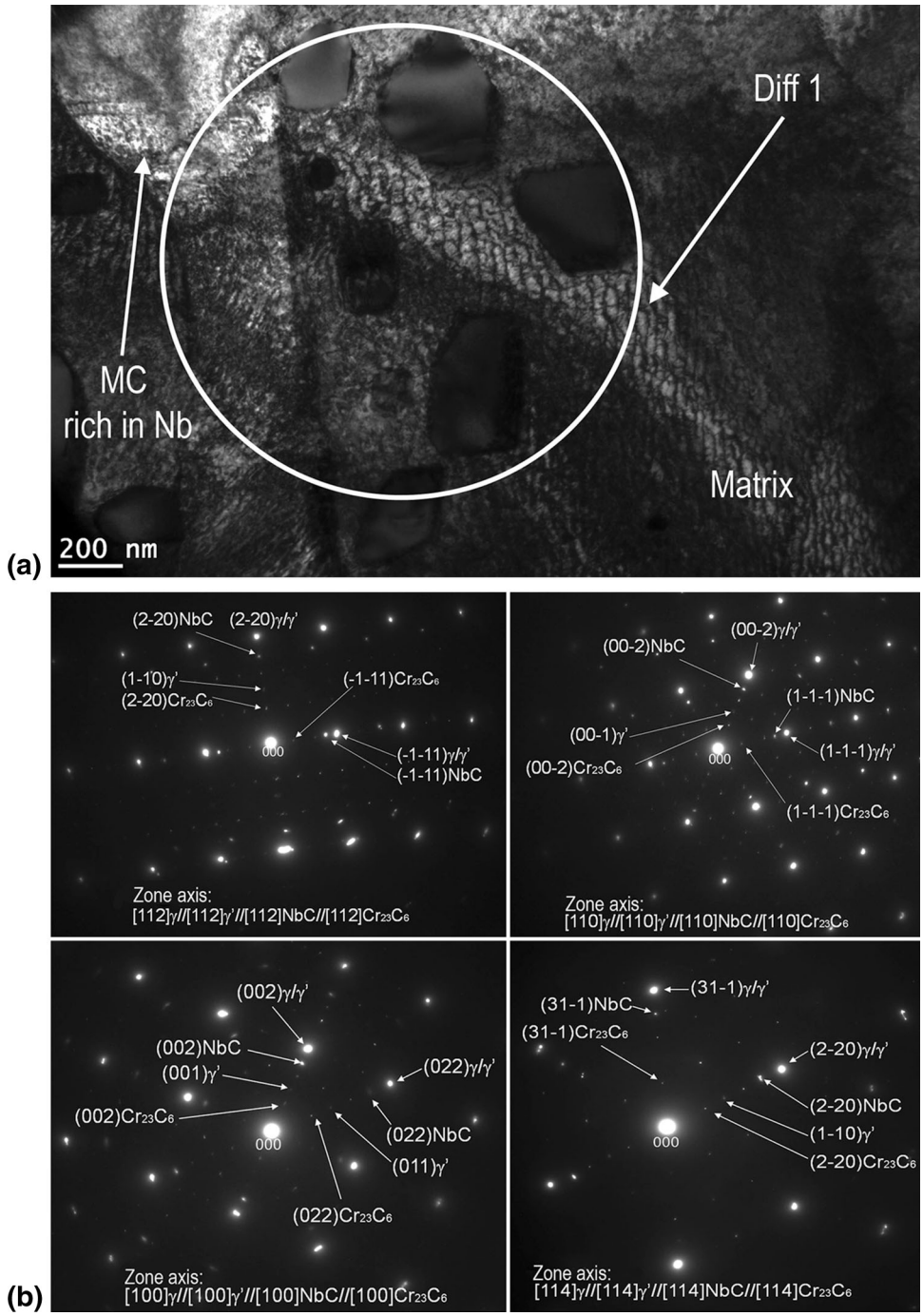

Fig. 5 TEM images in bright field of the microstructure of superalloy IN 713C in the area of NbC primary carbide dissolution (a) and the corresponding electron diffraction patterns (b)

According to the equilibrium system, Ni_7Zr_2 phase is formed directly from the liquid at 1420 °C. Next, at 1300 and 1180 °C, two peritectic reactions take place as follows: $L + Ni_7Zr_2 \rightarrow Ni_5Zr$ and $L + Ni_7Zr_2 \rightarrow Ni_{21}Zr_8$. It can be concluded that, at ambient temperature, no Ni_7Zr_2 phase occurs in the alloy eutectics. This phase might be present in the microstructure but not in the eutectic.

In order to explain the presence of phase Ni_7Zr_2 in the eutectic, we referred to the equilibrium systems of multi-element alloys. The results of the examinations of alloy Ni-7.9Al-7.7Cr-1.4Mo-1.7Zr-0.008B in (Ref 18) show that the microsegregation of the alloying elements during the solidification essentially changes the solidification path in the final stage. On the basis of our own research and the literature data (Ref 18-20), we conclude that in the first stage of solidification, γ phase crystals are formed. Next, with the decrease of temperature, the solubility of alloying elements (such as: Nb, Mo, Ti, C and B) in γ phase is reduced, which is manifested by their segregation at the γ phase dendrite—interdendritic liquid interface. Favorable conditions for the precipitation of primary carbides like NbC occur (according to the typical reaction $L \rightarrow \gamma + MC$) in interdendritic areas. These areas offer some

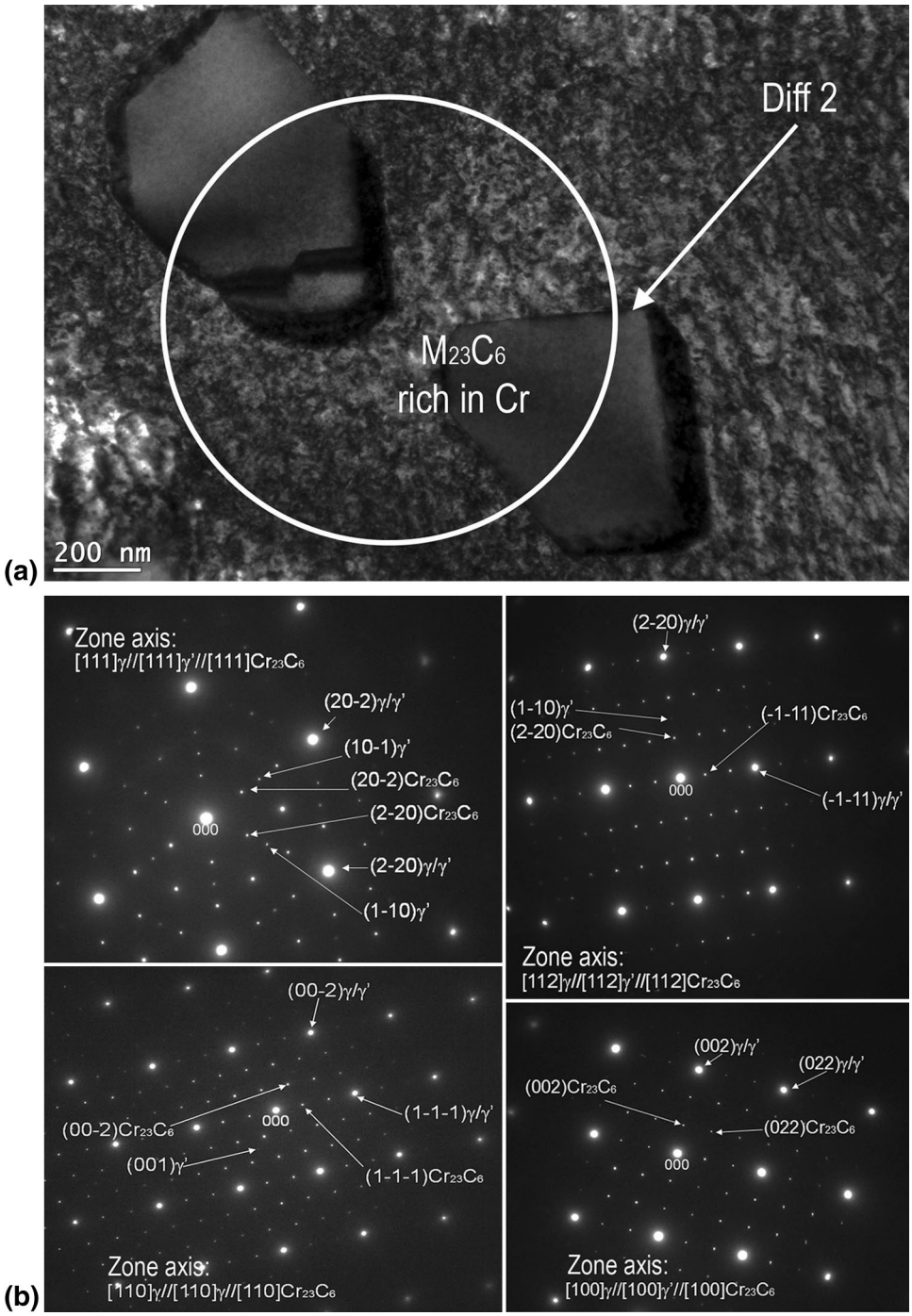

Fig. 6 TEM images in bright field of the microstructure of superalloy IN 713C in the area of $M_{23}C_6$ secondary carbide precipitation (a) and the corresponding electron diffraction patterns (b)

solubility of other carbide-forming elements, such as Ti, Mo, or Cr. The precipitation of the MC interdendritic liquid depletes these elements and enriches them with Al and Ti—the elements which are γ' formers.

In the final stage of solidification, we can thus observe a eutectic reaction $L \rightarrow \gamma + \gamma'$ in the areas where the interdendritic liquid is enriched with Al and Ti. The solubility of Zr and B in γ and γ' is extremely low, and thus, the latter segregates into the boundary eutectic (γ/γ')—residual liquid interface. The residual liquid rich in Zr reacts with the eutectic γ' phase according to the peritectic reaction $L + \gamma' \rightarrow \gamma + Ni_7Zr_2$ discussed in (Ref 18). This is followed by a eutectic reaction according to the formula $L \rightarrow \gamma + Ni_7Zr_2 + Ni_5Zr$. However, based on our own research, we did not confirm the presence of phase Ni_5Zr in the eutectic while the presence of borides M_3B_2 was proven. The research of Babu et al. (Ref 21) proved that, in the final stage of the alloy solidification, during the precipitation of γ/γ' eutectic, another reaction can occur, in which in the residual liquid enriched with Zr and B, a ternary eutectic is formed according to the reaction: $L \rightarrow \gamma + Ni_7Zr_2 + M_3B_2$.

Table 2 Comparison of the experimental $d_{(hkl)}$ spacing with the values from powder diffraction files, where: (a)PDF 47-1417; (b)PDF 18-0872; (c)PDF 74-1222; (d)PDF 85-1281; (e)PDF 18-0839; and (f)PDF 71-0543

(*hkl*)	γ	γ′	MC	$M_{23}C_6$	(*hkl*)	M_3B_2	(*hkl*)	Ni_7Zr_2
		$d_{(hkl)}$, Å				$d_{(hkl)}$, Å		$d_{(hkl)}$, Å
(111)	2.08 2.08(a)	2.08 2.06(b)	2.52 2.54(c)	6.13 6.15(d)	(001)	3.15 3.14(e)	(020)	4.05 4.12(f)
(100)	…	3.55 3.58(b)	…	…	(201)	2.14 2.13(e)	(−202)	2.28 2.26(f)
(110)	…	2.56 2.53(b)	…	…	(200)	2.90 2.87(e)	(−111)	3.98 3.95(f)
(200)	1.78 1.80(a)	1.78 1.79(b)	2.18 2.20(c)	5.33 5.33(d)	(211)	2.01 1.99(e)	(022)	3.37 3.41(f)
(220)	1.28 1.27(a)	1.28 1.27(b)	1.53 1.56(c)	3.83 3.77(d)	(010)	5.70 5.74(e)	(1−11)	3.79 3.76(f)
(311)	1.10 1.09(a)	1.10 1.08(b)	1.35 1.33(c)	3.26 3.21(d)	(310)	1.83 1.82(e)	(131)	2.32 2.34(f)

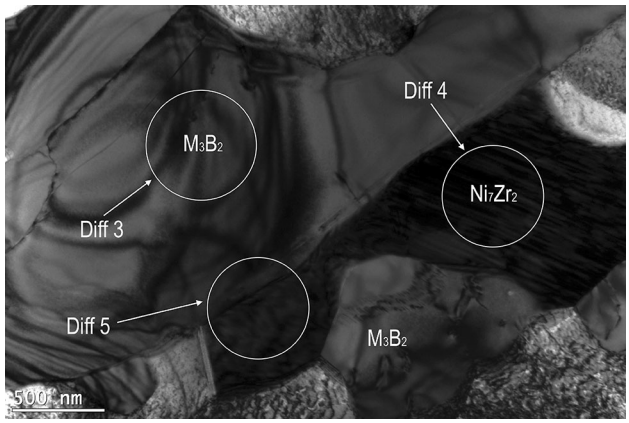

Fig. 7 Microstructure of superalloy IN 713C in the ($\gamma/Ni_7Zr_2/M_3B_2$) eutectic area

These results are in accordance with our observations. The $\gamma/Ni_7Zr_2/M_3B_2$ eutectic was observed both in the as-cast samples and after the stress rupture tests.

The presence of fine precipitations of M_3B_2 borides (which are not part of the eutectic mixture) and $M_{23}C_6$ secondary carbides observed after the stress rupture test can also be explained by the low solubility of B and C in the γ phase. In the austenitic steel of the 18Cr-15Ni type, at 1000 °C, the solubility of B in γ equals 0.004 wt.%, whereas at 800 °C, this value exceeds 0.002 wt.% (Ref 22). On the basis of the results presented in (Ref 23), it can be stated that, in the austenitic steel of the 18Cr-8Ni type, at 1000 °C, the solubility of C in γ equals 0.180 wt.%, and at 800 °C—it is 0.020 wt.% During the stress rupture test, the primary carbides undergo transformation, and thus, in the area of their decomposition, the γ phase solid solution becomes enriched with carbon. In connection with the fact that C has a lower atomic radius (76 pm) than B (84 pm), in the γ phase, it may dissolve in larger amounts than B. Thus, it reduces the solubility of B in γ, and at the ambient temperature, both borides and secondary carbides are precipitated. It has been shown in (Ref 24, 25) that borides (M_3B_2 and M_5B_3) and secondary carbides ($M_{23}C_6$ and M_6C) most often precipitate at the grain boundaries and phase interfaces.

Superalloys generally experience various microstructural changes during their service life, including γ′ coarsening (rafting), the precipitation of secondary carbides and borides, the topologically close-packed (TCP) phase formation, and the MC carbide degeneration (Ref 26-28). These processes remove many of strengthening elements from the γ matrix (e.g., Mo and Cr in the IN713C superalloy) and significantly degrade the properties of the superalloys, such as mechanical properties (tensile strength and creep resistance), corrosion resistance, and service life. Most of these features, such as γ′ coarsening/rafting, the precipitation of secondary carbides or borides, and TCP phases' formation, are reversible in the sense that, through heat treatments, one may restore microstructures and alloy properties to a practically "as-new" condition (Ref 26). However, primary MC decomposition is irreversible and might affect the aging process after the rejuvenated turbine parts are returned to service. Thus, in order to understand the MC degeneration better and to further upgrade the properties of superalloys, an extensive study in the field should be conducted.

5. Conclusions

On the basis of the obtained results, it can be concluded that the IN 713C superalloy undergoes significant degradation in the creep test at 980 °C under 150 MPa. The as-cast FCC matrix (γ phase solid solution, lattice constant a = 3.598 Å) is precipitation strengthened by coherent, ordered, and cubic $Ni_3(Al,Ti)$ γ′ phase (FCC ordered $L1_2$ crystal structure). In the interdendritic areas, there are precipitations of the NbC primary carbides (FCC with lattice constant a = 4.400 Å) and three eutectics: (γ/NbC), (γ/γ′), and ($\gamma/Ni_7Zr_2/M_3B_2$). Phase Ni_7Zr_2 has a monoclinic crystal structure (type of: mC36, C2/m12) with the lattice constants: a = 4.698 Å, b = 8.235 Å, c = 12.193 Å and the angle β = 95.93°. M_3B_2 borides possess tetragonal unit cells (type of: tP10, F4/mbm) with the lattice constants $a = b$ = 5.775 Å and c = 3.145 Å.

After the creep test, we observed a directional growth (rafting) of γ′ phase in the matrix as well as decomposition of NbC carbides. As a result of MC decomposition, secondary carbides rich in Cr, $M_{23}C_6$ were precipitated (FCC unite cell with lattice constant a = 10.660 Å) as well as the γ′ phase. It was also shown that the process of secondary carbide precipitation can be accompanied by the precipitation of M_3B_2 borides rich in Mo.

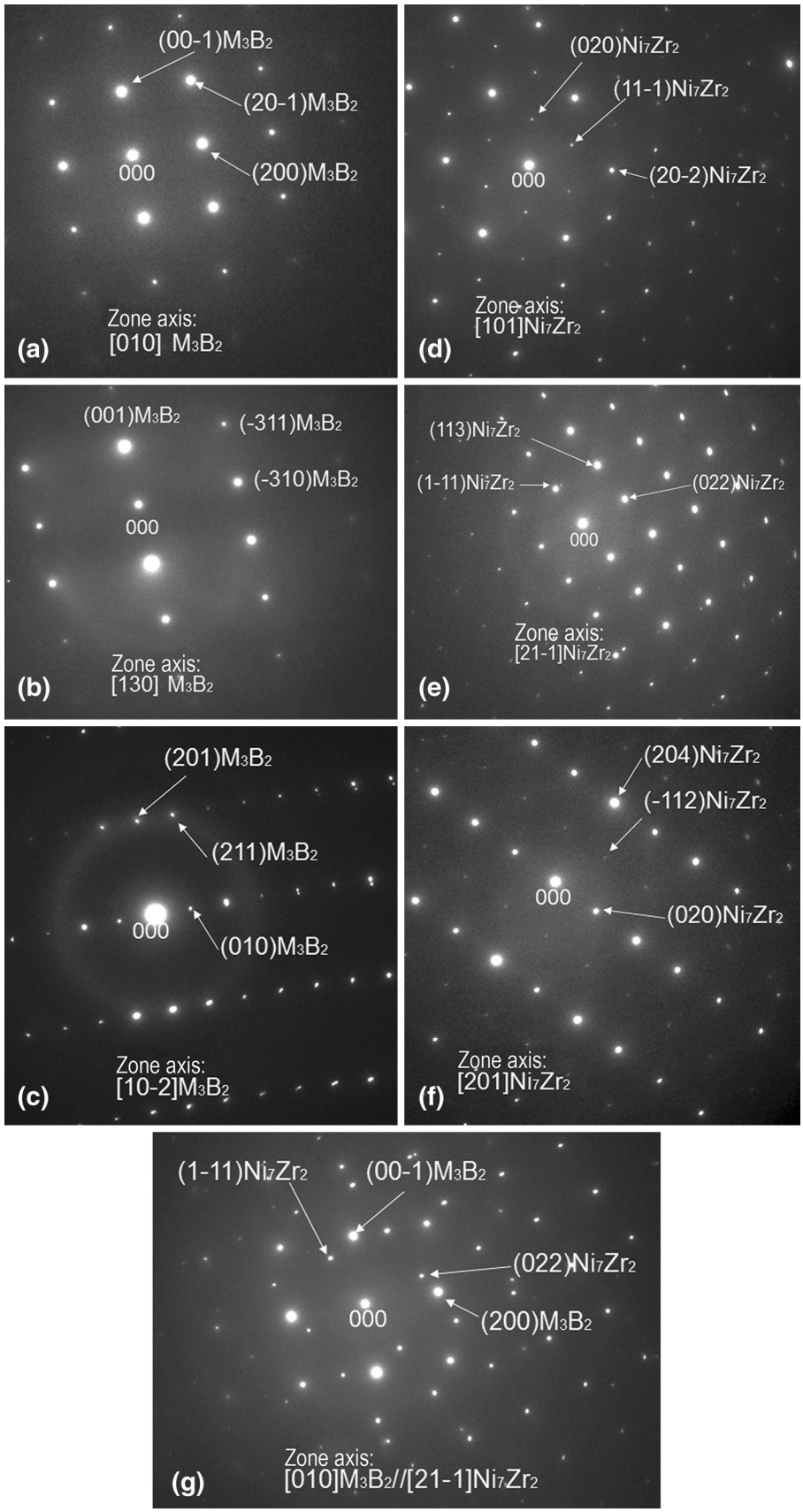

Fig. 8 Electron diffraction patterns corresponding to the analysis areas shown in Fig. 7, where (a-c) is area 3; (d-f) is area 4; and (g) is area 5

Acknowledgments

This research was financed from the public resources of the Polish National Centre for Research and Development; the project was implemented within the frames of the Program INNOTECH-K2/IN2/8/181849/NCBR/13, program path IN-TECH.

References

1. J.R. Brinegar, J.R. Mihalisin, and J. VanderSluis, The effect of Tantalum for Columbium Substitutions in Alloy 713C, *Proc. Int. Symp. Super.*, 1984, p 53–62
2. F. Zupanic, T. Boncina, A. Krizman, and F.D. Tichelaar, Structure of Continuously cast Ni-Based Superalloy Inconel 713C, *J. Alloy. Compd.*, 2001, **329**, p 290–297
3. A.K. Bhambri, T.Z. Kattamis, and J.E. Morral, Cast Microstructure of Inconel 713C and its Dependence on Solidification Variables, *Metall. Trans. B*, 1975, **6B**, p 523–537
4. A. Somoza, G. Santos, A. Ges, R. Versaci, and F. Plazaola, Age-Hardening and Precipitation Phenomena in the Inconel-713C Superalloy Studied by Means of Positron Lifetime Spectroscopy, *Phys. Status Solid A*, 1999, **174**(1), p 189–198
5. A. Ges, H. Palacio, and R. Versaci, IN-713C Characteristic Properties Optimized Through Different Heat Treatments, *J. Mater. Sci.*, 1994, **29**, p 3572–3576
6. M. Lachowicz, W. Dudziński, K. Haimann, and M. Podrez-Radziszewska, Microstructure Transformations and Cracking in the Matrix of γ-γ′ Superalloy Inconel 713C Melted with Electron Beam, *Mater. Sci. Eng. A*, 2008, **479**, p 269–276
7. M. Lachowicz, W. Dudziński, and M. Podrez-Radziszewska, TEM Observation of the Heat-Affected Zone in Electron Beam Welded Superalloy Inconel 713C, *Mater. Charact.*, 2008, **59**, p 560–566
8. M.B. Lachowicz, Microstructural Changes in Padding Welds Made from the 713C Alloy After Heat Treatment, *Arch. Foundry Eng.*, 2010, **10**(3), p 11–16
9. U. Brandt and C.M. Sonsino, Lebensdauervorhersage fur integralgegossene Turbinenrader unter Berucksichtigung kurzer Risse am Beispiel der Nickelbasis-Legierung IN 713C, *Mat.-wiss. u. Werkstofftech.*, 1995, **26**, p 294–308
10. M. Kamaraj, C. Mayr, M. Kolbe, and G. Eggeler, On the Influence of Stress State on Rafting in the Single Crystal Superalloy CMSX-6 Under Conditions of High Temperature and Low Stress Creep, *Scr. Mater.*, 1998, **38**(4), p 589–594
11. T. Tinga, W.A.M. Brekelmans, and M.G.D. Geers, Directional Coarsening in Nickel-Base Superalloys and its Effect on the Mechanical Properties, *Comput. Mater. Sci.*, 2009, **47**, p 471–481
12. F. Touratier, E. Andrieu, D. Poquillon, and B. Viguier, Rafting Microstructure During Creep of the MC2 Nickel-Based Superalloy at Very High Temperature, *Mater. Sci. Eng. A*, 2009, **510–511**, p 244–249
13. L. Kommel, E. Kimmari, M. Viljus, R. Traksmaa, O. Volobueva, and I. Kommel, Phases Micromechanical Properties of Ni-Base Superalloy Measured by Nanoindentation, *Mater. Sci. (Medziag.)*, 2012, **18**(1), p 28–33
14. H. Matysiak, M. Zagorska, J. Andersson, A. Balkowiec, R. Cygan, M. Rasinski, M. Pisarek, M. Andrzejczuk, K. Kubiak, and K.J. Kurzydlowski, Microstructure of Haynes® 282 ® Superalloy After Vacuum Induction Melting and Investment Casting of Thin-Walled Components, *Materials*, 2013, **6**, p 5016–5037
15. C.T. Sims, N.S. Stoloff, and W.C. Hagel, *Superalloys II*, John Wiley & Sons, New York, NY, 1987
16. ASM International. Handbook Committee. *Nickel, Cobalt and Their Alloys*; J.R. Davis, Ed., ASM International, Almere, 2000
17. P. Nash and C.S. Jayanth, The Ni-Zr (Nickel-Zirconium) System, *Bull. Alloy Phase Diagr.*, 1984, **5**(2), p 144–147
18. H.B. Motejadded, M. Soltanieh, and S. Rastegari, Dissolution Mechanism of a Zr rich Structure in a Ni_3Al Base Alloy, *J. Mater. Sci. Technol.*, 2011, **27**(10), p 885–892
19. O.A. Ojo, N.L. Richards, and M.C. Chaturvedi, Microstructural Study of Weld Fusion Zone of TIG Welded IN 738LC Nickel-Based Superalloy, *Scr. Mater.*, 2004, **51**, p 683–688
20. R.K. Sidhu, O.A. Ojo, and M.C. Chaturvedi, Sub-solidus Melting of Directionally Solidified Rene 80 Superalloy During Solution Heat Treatment, *J. Mater. Sci.*, 2008, **43**, p 3612–3617
21. S.S. Babu, S.A. David, J.M. Vitek, and M.K. Miller, Atom-Probe Field-Ion Microscopy Investigation of CMSX-4 Ni-Base Superalloy Laser Beam Welds, J. Phys. IV France 06 (1996) C5-253–C5-258, *International Field Emission Society IFES'96 Proceedings of the 43rd International Field Emission Symposium*
22. J.P. Hoffman and A.S.M. De Jesus, The Distribution of Boron in Stainless Steels as Revealed by a Nuclear Technique, *J. S. Afr. Inst. Min. Metall.*, 1989, **89**(3), p 81–87
23. S.J. Rosenberg and C.R. Irish, Solubility of Carbon in 18-Percent-Chromium-10-Percent-Nickel Austenite, *J. Res. Natl. Bur. Stand.*, 1952, **48**(1), p 40
24. H.R. Zhang, O.A. Ojo, and M.C. Chaturvedi, Nanosize Boride Particles in Heat-Treated Nickel Base Superalloys, *Scr. Mater.*, 2008, **58**, p 167–170
25. L.O. Osoba, R.G. Ding, and O.A. Ojo, Improved Resistance to Laser Weld Heat-Affected Zone Microfissuring in a Newly Developed Superalloy Haynes 282, *Metall. Mater. Trans. A*, 2012, **43A**, p 4281–4295
26. G. Lvov, V.I. Levit, and M.J. Kaufman, Mechanism of Primary MC Carbide Decomposition in Ni-Base Superalloys, *Metall. Mater. Trans. A*, 2004, **35A**, p 1669–1679
27. X.Z. Qin, J.T. Guo, C. Yuan, C.L. Chen, and H.Q. Ye, Effects of Long-Term Thermal Exposure on the Microstructure and Properties of a Cast Ni-Base Superalloy, *Metall. Mater. Trans. A*, 2007, **38A**, p 3014–3022
28. X.Z. Qin, J.T. Guo, C. Yuan, C.L. Chen, J.S. Hou, and H.Q. Ye, Decomposition of Primary MC Carbide and its Effects on the Fracture Behaviors of a Cast Ni-Base Superalloy, *Mater. Sci. Eng. A*, 2008, **485**, p 74–79